ELSEVIER

Journal of Power Sources 93 (2001) 112–122

JOURNAL OF POWER SOURCES

www.elsevier.com/locate/jpowsour

Heat dissipation in a lithium ion cell

Hari Vaidyanathan[a,*], William H. Kelly[b], Gopalakrishna Rao[c]

[a]*COMSAT Laboratories, Clarksburg, MD, USA*
[b]*William H. Kelly & Associates, Gaithersburg, MD, USA*
[c]*NASA Goddard Space Flight Center, Greenbelt, MD, USA*

Received 8 July 2000; accepted 2 August 2000

Abstract

A comparative study of the heat dissipated by a 3.3 A h $Li_xC/LiNiO_2$ cell and a 1.25 A h $Li_xC/75\%$ $LiCoO_2$, 25% $LiNiO_2$ cell was conducted through experimental heat rate measurements using a radiative calorimeter. The specific heat of the cell was determined experimentally to be 0.969 J/°C g for the $LiNiO_2$ cell and 0.946 J/°C g for the $Li_xC/75\%$ $LiCoO_2$, 25% $LiNiO_2$ cell. The $Li_xC/LiNiO_2$ cell had a higher self-discharge rate than the $Li_xC/75\%$ $LiCoO_2$, 25% $LiNiO_2$ cell. The heat dissipated during discharge increased with the rate of discharge. During charge, initial endothermic cooling and subsequent exothermic heating beyond 55% state-of-charge were observed. At the *C*/2 rate of discharge (medium rate), the heat dissipated was 17 mW/cm^3 for the $Li_xC/LiNiO_2$ cell and 11.2 mW/cm^3 for the $Li_xC/75\%$ $LiCoO_2$, 25% $LiNiO_2$ cell. The experimental values obtained for the heat dissipation at various charge and discharge rates were used to calculate thermoneutral potentials of 3.698 and 3.836 V for the $Li_xC/LiNiO_2$ and $Li_xC/75\%$ $LiCoO_2$, 25% $LiNiO_2$ cells, respectively. The proposed values for thermoneutral potential may explain the endothermic cooling during charge and the negative temperature coefficient for cell voltage.

Keywords: Heat dissipation; Lithium ion cell; Radiative calorimeter

1. Introduction

A commercial lithium ion battery that uses the ''rocking chair'' concept (in which the lithium ions ''rock'' from one state (cathode) to another (anode)) was introduced in 1990 [1] and has gained wide acceptance for a range of applications due to attractive features such as high voltage, light weight, and small dimensions. The battery consists of a carbon anode and a lithiated metal-oxide cathode in an aprotic solvent containing a dissolved lithium salt [2]. There is no metallic lithium in the cell. The cell voltage results from the difference in the activity of lithium ions in the carbon anode and lithium nickel oxide (or cobalt oxide) cathode. Performance features such as the variation of capacity with temperature and rate of discharge, self-discharge, voltage profiles, and cycle life have been discussed at length by various authors [3,4]. The cathode is the source of the lithium ions and is depleted to a value corresponding to $Li_{0.35}NiO_2$ or $Li_{0.5}CoO_2$ during charge. Cell voltage increases with increase in the state of charge, and at the charge termination voltage of 4.1 V, the anodic composition corresponds to $Li_{0.8}C_6$. The cell shows a mid-discharge voltage of 3.5 V, which decreases as a function of the voltage termination value during charge. The cell cannot be overcharged or overdischarged. It undergoes self-discharge at a rate that is a function of temperature, anode structure, and the formulation of the electrolyte. The rate is lower than that occurring in conventional alkaline rechargeable batteries.

Heat dissipation during discharge, charge, and self-discharge of batteries is an important parameter not only for the safe operation of the battery but also for extending its cycle and calendar life. In addition, the battery is susceptible to thermal runaway when heat is generated faster than it can be dissipated. Another thermal condition that affects the operation of the battery is the development of thermal gradients and hot spots, which greatly accelerates the degradation of the electrolyte, anode, cathode, and separator.

The thermal characterization of lithium ion cells is more complex and fraught with difficulties due to uncertainty regarding enthalpy values, reaction mechanisms, and side reactions. The side reactions that contribute to exothermic heating or endothermic cooling are the corrosion of copper, dissolution of lithium nickel-oxide and lithium cobalt-oxide, polymerization of the electrolyte, production of gases such as ethylene, propylene, hydrogen, and oxygen, and the hydration and formation of carbonates and fluorides. Mathematical analysis of heat rates for lithium ion cells has been

* Corresponding author. Tel.: +1-301-428-4007; fax: +1-301-428-7747.
E-mail address: hari.vaidyanathan@comsat.com (H. Vaidyanathan).

0378-7753/01/$ – see front matter
PII: S0378-7753(00)00550-4

reported by Chen and Evans [5], calorimetric measurements of heat rates by Hong et al. [6] and thermodynamic calculations by Deiss et al. [7]. In [5–7], the authors report that the temperature coefficient of cell open-circuit voltage is −0.4 mV/K, the heat dissipation rate during *C*/2 discharge is 10 mW/cm^3, thermal runaway does not occur during normal battery operation, entropic heat is more than 50% of the total heat and increases with increase in the rate of discharge, and there is a divergence in the calculated and measured values for the open-circuit potential.

The present study was conducted to determine the heat dissipation rates from $Li_xC/LiNiO_2$ and Li_xC/75% $LiCoO_2$, 25% $LiNiO_2$ cells during charge and discharge, and then to measure thermal capacity and calculate thermoneutral potential as a function of state of charge. The experimental approach used a radiative calorimeter, and the measurements were performed under transient conditions. The radiative calorimeter is ideally suited for determining the heat rates of fractional watts because of its high sensitivity, which is 0.002 W/°C for the radiative term, compared to 1 W/°C for the calorimetric constant for the conductive calorimeter. Heat leakage through the leads and sensing wires by conduction can be calculated and compensated. Heat stored and heat dissipated are calculated separately.

2. Cell selection

The cells selected for this study were provided to NASA Goddard Space Flight Center for an evaluation program. The $Li_xC/LiNiO_2$ cell was a cylindrical 3.7 A h cell fabricated in a stainless steel can containing a graphite anode with a glass-to-metal seal, polypropylene separator, and an electrolyte formulation consisting of $LiPF_6$ dissolved in a mixture of ethylene carbonate (EC) and dimethyl carbonate (DMC). The Li_xC/75% $LiCoO_2$, 25% $LiNiO_2$ cell had a capacity of 1.25 A h and contained the same type of graphite as the anode material, separator, and electrolyte, with a plastic-insulated seal and a puncture diaphragm, in a nickel-plated can. The dimensions were those of a type-18650 cell. Both cell types contained spirally wound electrodes of different lengths and diameters.

3. Calorimeter

The calorimeter is designed for radiative transfer of heat from the cell to its surroundings [8]. It consists of a 0.5 m^3 copper chamber that is maintained at −168°C by circulating liquid nitrogen. The inside of the chamber is painted black, and the cell is suspended using a lacing cord. The calorimetric chamber is arranged in a bell-jar-type (45 cm diameter and 73 cm tall) vacuum chamber, and a vacuum of 10^{-5} Torr is maintained.

In preparing the cell for calorimetry, great care was taken to see that it had a distinct radiating surface. A 2.54 cm-wide thermofoil heater tape was wrapped around the cell and bonded to the cell case by means of epoxy. The heater taped area constituted the radiating surface, which was 26.7 cm^2 for the $LiNiO_2$ cell and 12.9 cm^2 for the $LiNiO_2$ cell. Six thermocouples were installed at different areas of the cell, with care being taken not to contact any of the thermocouples to the thermofoil heater. The thermocouples were distributed as follows: one at the cell cover, one at the bottom of the can, and four on the cylindrical region of the can. The thermocouple sensing wires, terminal leads, voltage sensing leads, and heater leads were bunched to create a wire bundle and insulated with multiple layers of aluminized Mylar. The exposed areas of the cell were also insulated with multiple layers of Mylar. The Mylar insulation is required to prevent heat loss through radiation from any surface other than the area wrapped with the heater tapes. A thermocouple was attached to the calorimeter chamber to ascertain the flow of liquid nitrogen. Another thermocouple was attached to the end of the wire bundle under the Mylar insulation before it exited the chamber, so that the temperature reading could be used to calculate heat transferred by conduction. Fig. 1 shows the test configuration for the cell. Heat was applied to the cell through the thermofoil heaters in order to raise the cell temperature significantly above that of the calorimetric chamber (−168°C). Thus, heat is radiated from the cell and follows the relationship

$$Q_r = \varepsilon\sigma(T_c^4 - T_s^4) \quad (1)$$

where Q_r is the heat radiated (W), ε the emissivity, σ the Stefan–Boltzmann constant (5.667×10^{-8} W/m^2 K), T_c the temperature of the cell (°C) and where T_s is the temperature of the calorimeter (105 K).

The radiative calorimetry determined the following:

1. *Heater power setting*: an approximate calculation of the heater power required to maintain the cell from −5 to 30°C, using Eq. (1).
2. *Calibration and heat radiated, Q_r*: a determination of steady-state temperatures for various values of applied heater power, and curve-fitting of the data to derive an expression for Q_r.
3. *Thermal capacity, C_p*: determined based on transient cooling and warm-up curves.
4. *Conductive heat loss*: the heat associated with conduction through the lead and sensing wires is calculated using

$$Q_{cond} = \frac{hA(T_c - T_{wire\ bundle})}{L} \quad (2)$$

where Q_{cond} is the heat transfer by conduction (W), h the effective thermal conductivity (W/cm °C) with the values used being 3.75 W/cm K for copper and 0.21 W/cm K for constantan, A the cross-sectional area (cm^2), T_c the temperature of the cell (°C), $T_{wire\ bundle}$ the temperature of the wire bundle (°C) and where L is the length of wires and leads (cm).

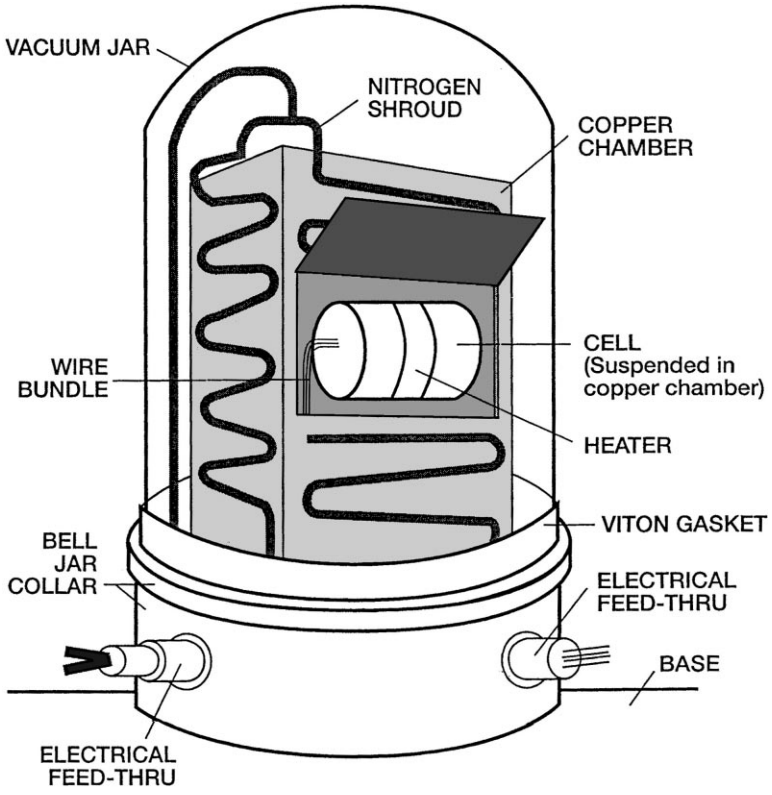

Fig. 1. Test schematic.

5. *Rate of energy stored,* Q_s: this is calculated using

$$Q_s = \frac{mC_p\delta T}{\delta t} \quad (3)$$

where Q_s is the rate of energy stored (W), m the mass of the cell (g), C_p the specific thermal capacity of the cell (J/°C), δT_c the temperature change of the cell (°C) and where δt is the elapsed time (s).

6. *Heat dissipated from the cell,* Q_{diss}: the rate of heat dissipation from the cell is determined as follows:

$$Q_{diss} = Q_h - Q_r - Q_{cond} - Q_s \quad (4)$$

where Q_h is the heater power in watts.

The test conditions and values for the various parameters are given in Table 1.

The function of the calorimeter described above differs markedly from that of conventional conductive calorimeters. Conductive calorimetry is performed under both steady-state and dynamic conditions. In the steady-state technique, the term $mC_p\delta T/\delta t$ is not used in the calculations. The conduction term is

$$Q_{cond} = hA(T_{cell} - T_{cal}) \quad (5)$$

where h is the heat transfer coefficient (W/cm °C), A the surface area of the cell (cm^2), T_{cell} the cell surface temperature (°C) and where T_{cal} is the calorimeter temperature (°C).

Table 1
Test conditions

Parameter	Value
Calorimeter size	0.5 m^3, copper chamber
Calorimeter temperature	−168°C
Calorimeter pressure	10^{-5} Torr
Heat transfer mode	Radiation
Cell temperature	Average of three thermocouples located on the cell surface for the $LiNiO_2$ cell (two for the $LiCoO_2$ cell)
Conductive correction	Heat transfer through the wire bundle is included in the calculation
Heater tape	Nichrome, 12.9 cm^2
Data intervals	60 s
Charge/discharge	Constant current
Voltage limits	4.1 V for charge termination
	2.5 V for discharge termination

In this technique, radiation is neglected. The minimum heat that can be measured is 38 mW/°C, as stated in [6].

Radiative calorimetry, on the other hand, is performed in an environment where radiation is the major mode of heat transfer. The apparatus is simple, and the minimum heat that can be measured can be varied by adjusting the area of the radiating surface. The equivalent calorimetric constant is 1.8 mW/°C. The resolution can be increased by decreasing the area of the radiating surface (by insulating most of the cell surface with multiple layers of aluminized Mylar). Radiative calorimetry is a transient technique ideally suited to determining the heat dissipated from a cell during charge and discharge. The main sources of error are the curve-fitting to obtain Q_r, temperature, heater power, and heat leakage through the insulation.

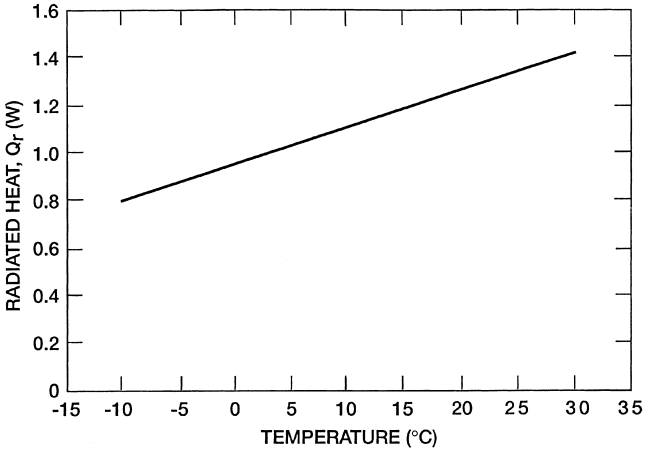

Fig. 2. Variation of radiated heat with cell temperature.

4. Calibration

The power applied to the cell heater was set at several different values and the corresponding cell temperatures were measured at steady state and at open-circuit voltage. The cell temperature is determined based on an average of the values taken from two thermocouples mounted on the cylindrical surface of the cell. To allow for heat loss and gain through the voltage-sensing and power leads, heater power leads, and thermocouple leads, the conductive heat transfer from the cell through the leads was calculated by measuring the temperature difference at the beginning (cell surface) and end (point of exit from the calorimeter) of the wire bundles and inserting the values for the length and cross-section of the wires into Eq. (2). The calculated Q_{cond} was 0.00137 W/°C for the $Li_xC/LiNiO_2$ cell and 0.01118 W/°C for the $Li_xC/75\%$ $LiCoO_2$, 25% $LiNiO_2$ cell. The value for Q_{cond} is higher for the $Li_xC/75\%$ $LiCoO_2$, 25% $LiNiO_2$ cell due to the increased number of sensor wires and their shorter length. The calculated Q_{cond} is deducted from the heater power to obtain Q_r. Then, a steady-state curve is constructed by plotting the average temperature of the cell against Q_r. Fig. 2 shows the plot obtained for the 75% $LiCoO_2$, 25% $LiNiO_2$ cell. A similar plot was obtained for the $LiNiO_2$ cell. The following equations were then derived by curve-fitting:

$$Q_r = 1.675 \times 10^{-10}(273 + T_{avg})^4 \quad \text{for the } Li_xC/75\%\,LiCoO_2, 25\%\,LiNiO_2 \text{ cell} \tag{6}$$

$$Q_r = 1.55 \times 10^{-10}(273 + T_{avg})^4 \quad \text{for the } Li_xC/LiNiO_2 \text{ cell} \tag{7}$$

where Q_r is the heat radiated, in watts, and T_{avg} is the average of readings from the thermocouples installed on the cell.

5. Thermal capacity

The importance of using accurate values for thermal capacity in any thermal calculation is well documented. In this study, the thermal capacities for the cells were determined experimentally since the mass and specific heat of the various components in the cells were not known with certainty.

The thermal capacity of the $Li_xC/LiNiO_2$ cell was determined from the temperature transients observed during warm-up at a heater power of 2.51 W, and during cool-down using no heater power. The average cell temperature was converted to Q_r using Eq. (6) for several time intervals, and Q_{cond} was calculated using Eq. (2). The thermal capacity was then calculated using

$$MC_p = (Q_h - Q_r - Q_{cond})\frac{\delta t}{\delta T} \tag{8}$$

The specific thermal capacity of the $Li_xC/LiNiO_2$ cell was 111.5 J/°C, and the normalized value was 0.969 J/°C g. The specific thermal capacity of the cell can also be calculated from the approximate mass and specific heat of cell components such as graphite, $LiNiO_2$, EC, DMC, $LiPF_6$, stainless steel, copper, aluminum, and polypropylene. Precise values for mass and specific heat are not known; however, an approximation from the data provided by the cell manufacturer regarding the components and their mass gave a value of 102 J/°C for thermal capacity for the $LiC/LiNiO_2$ cell, which compares well with the experimental value.

The thermal capacity of the $Li_xC/75\%$ $LiCoO_2$, 25% $LiNiO_2$ cell was determined from the temperature transients observed during warm-up at a heater power of 1.92 W, and during cool-down. The specific thermal capacity of the cell was 40.246 J/°C, and the normalized value was 0.946 J/°C g.

6. Electrochemical characteristics

The impedance of the $LiNiO_2$ cell was measured at 1 kHz, and a value of 110 mΩ was obtained. The cell was stabilized at several temperatures by applying the proper heater power (using the calibration curve as a guide) and subjected to several charge and discharge capacity determination cycles

Table 2
Electrochemical properties

Parameter	$LiNO_2$ cell	75% $LiCoO_2$, 25% $LiNiO_2$ cell
Mass (g)	115	42.57
Volume (cm^3)	50.81	16.54
Diameter (cm)	3.4	1.8
Height (cm)	5.1	6.5
Electrical capacity (A h)		
0°C, *C*/5 rate	2.49	0.945
10°C, *C*/5 rate	3.09	1.162
25°C, *C*/5 rate	–	1.277
25°C, *C*/2 rate	3.791	1.252
35°C, *C*/5 rate	3.884	–
Impedance (mΩ)	110	130
Self-discharge in 72 h (%)	4.9	3.39

at various rates and temperatures. The charging was done at constant current with a voltage limit of 4.1 V, and the discharging at constant current to a voltage limit of 2.5 V. The cell had a capacity of 3.88 A h at a discharge rate of 1 A at 35°C, with a mid-discharge voltage of 3.49 V (taken at the midpoint of the discharge duration). The capacity decreased with decrease in temperature and increase in the rate of discharge. The capacity remaining in a charged cell after 72 h in the open-circuited condition at 10°C was 3.041 A h, which translated to a loss of 4.9%. The loss for an Ni–Cd battery under the same conditions is 10%. Table 2 summarizes the capacity, impedance, and self-discharge data obtained.

The performance features of the 75% $LiCoO_2$, 25% $LiNiO_2$ cell are characterized by a capacity of 1.27 A h at 25°C and a mid-discharge voltage of 3.6 V. The capacity loss due to self-discharge in the 72 h stand test was 3.39%. Cell impedance was 130 mΩ. Fig. 3 shows the voltage profiles obtained during the *C*/5 rate of charge for the Li_xC/75% $LiCoO_2$, 25% $LiNiO_2$ cell, and during the *C*/7 rate for the $Li_xC/LiNiO_2$ cell. Fig. 4 shows the voltage profiles during the *C*/4 rate for the $Li_xC/LiNiO_2$ cell, and at the *C*/2 and *C*/5 rates for the Li_xC/75% $LiCoO_2$, 25% $LiNiO_2$ cell discharge. Note that the voltage profiles show lower voltages during charge and discharge for the $Li_xC/LiNiO_2$ cell. The variation of cell voltage with state of charge followed the general trend published in the literature.

7. Heat dissipation during charge

The power applied to the cell heater was adjusted in order to stabilize the cell at 25°C. The Li_xC/75% $LiCoO_2$, 25% $LiNiO_2$ cell was charged at 250 mA to 4.1 V, after stabilizing at a heater power of 1.912 W, and values for Q_r, Q_s, and Q_{diss} were determined at 1 min intervals. Fig. 5 shows the voltage and Q_{diss} (heat rate profile). The thermal behavior of the cell is characterized by an initial rise in heat dissipation, followed by a minimum and endothermic cooling at about 25–30% state-of-charge, and a leveling-off towards the end of charge. The maximum endothermic rate is 0.015 W. At the end of charge, Q_{diss} is 0.039 W.

Fig. 6 shows the temperature profile during charge at 250 mA. The temperature curve shows an inflection corresponding to endothermic cooling at about 25–30% state-of-charge and levels off toward the end of charge.

The charging reactions consist of intercalation of lithium ions to the graphite anode and deintercalation from the nickel-oxide cathode. The entropy change dominates the total heat dissipated during charge at *C*/5. The deintercalation from the cathode is believed to be endothermic. (Reactions at the carbon anode are not expected to be of any thermal consequence.)

The $LiNiO_2$ cell was stabilized at 0°C and charged at a constant current of 400 mA. Temperature and heat dissipa-

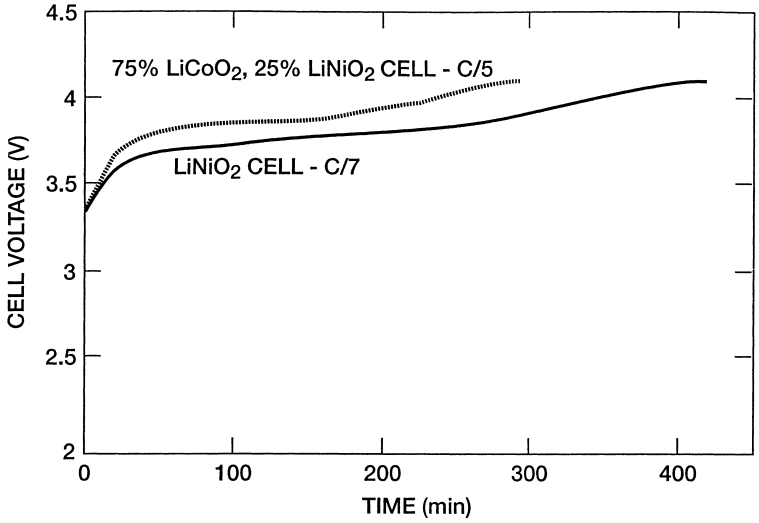

Fig. 3. Voltage profiles obtained during charge for the $LiNiO_2$ and 75% $LiCoO_2$, 25% $LiNiO_2$ cells.

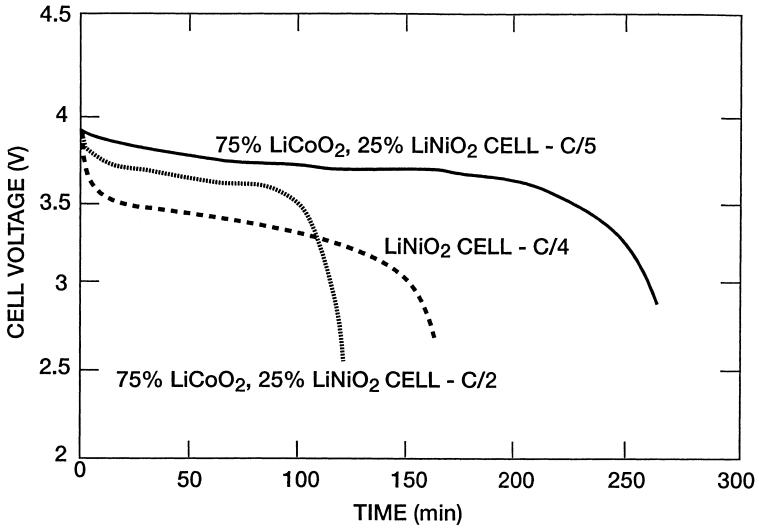

Fig. 4. Voltage profiles obtained during discharge for the $LiNiO_2$ and 75% $LiCoO_2$, 25% $LiNiO_2$ cells.

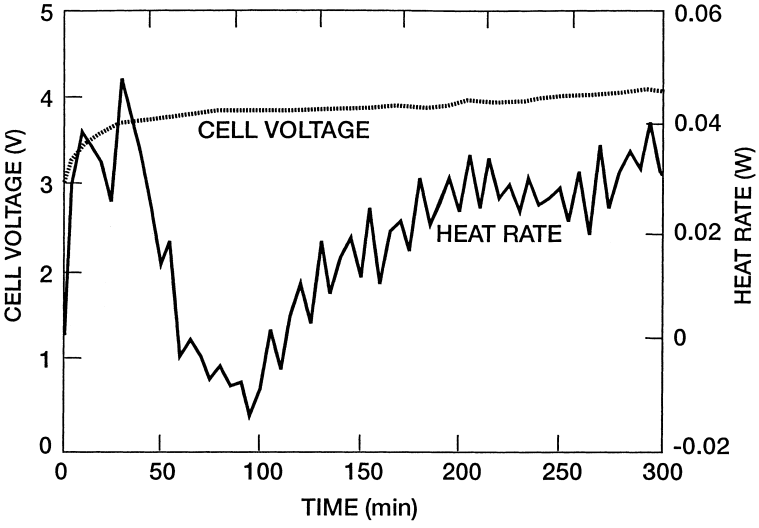

Fig. 5. Variation of heat rate during charge at *C*/5 for the 75% $LiCoO_2$, 25% $LiNiO_2$ cell.

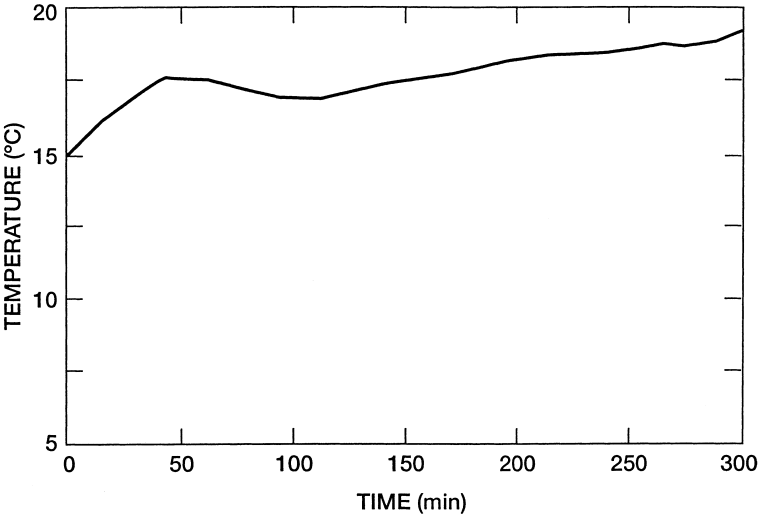

Fig. 6. Variation of temperature during charge at *C*/5 for the 75% $LiCoO_2$, 25% $LiNiO_2$ cell.

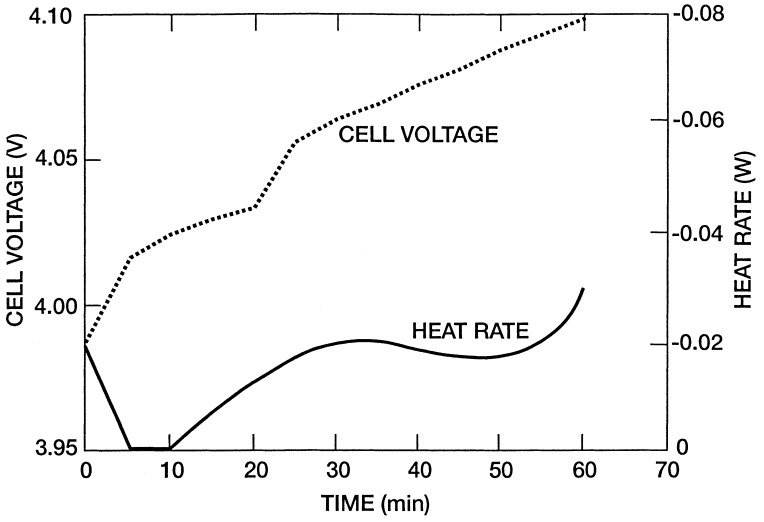

Fig. 7. Variation of heat dissipation and voltage during trickle charge at 0.06 A for the $LiNiO_2$ cell.

tion were monitored continuously until the voltage reached 4.1 V. The average heat dissipation rate was 0.064 W, or 0.00082 W/cm^2 of the surface area of the cell. The normalized heat rate was 0.0012 W/cm^3. Heat dissipation increased rapidly at the beginning of charge, and then leveled off before rising towards the end of charge.

At the conclusion of the 400 mA charge, the cell was trickle-charged at 60 mA and the rate of heat dissipation was determined. Fig. 7 shows the variation in heat rate and voltage over time, and Fig. 8 shows the variation in voltage and temperature over time. The cell voltage increased during trickle charge and reached the limit of 4.1 V in 1 h. The values for the heat rate are shown as negative numbers to indicate its endothermic effect. The tendency for the heat rate to increase rapidly towards the end of the 400 mA charge was not apparent, and endothermic cooling began, with a cooling rate of 0.0002 W/cm^2. The cell temperature showed a marginal decrease of 0.2°C. The state of charge of the cell increased further during trickle charge. The observation of marginal cooling during trickle charge is interesting and can be used to advantage in the charging scheme for aerospace applications.

8. Heat dissipation during discharge

The heat dissipation during discharge at different rates for the 75% $LiCoO_2$, 25% $LiNiO_2$ cells under test is shown in Fig. 9. The profiles show an initial maximum in the heat rate, followed by a minimum. This initial increase has also been reported by Hong et al. [6]. The maximum heat rate during 625 mA (*C*/2) discharge was 0.28 W, and at 1.25 A (*C*) rate, it was 0.55 W. Thus, at a medium rate of discharge, heat dissipation was 11.21 mW/cm^3, which is lower than that

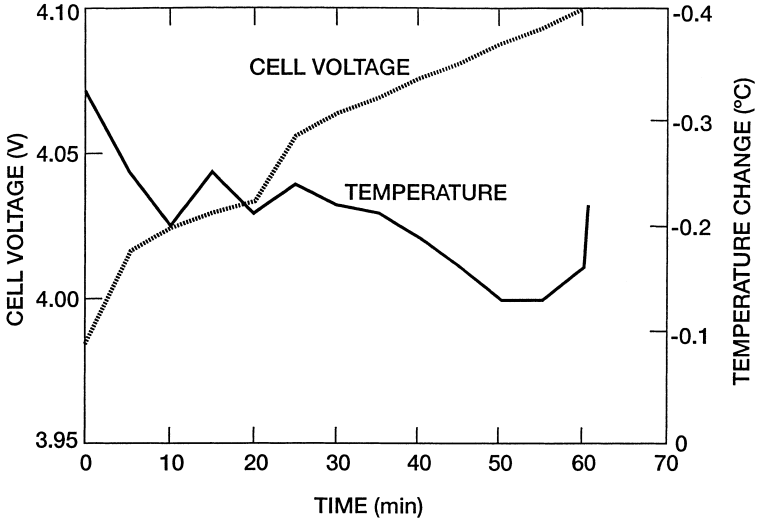

Fig. 8. Variation of temperature and voltage during trickle charge at 0.06 A for the $LiNiO_2$ cell.

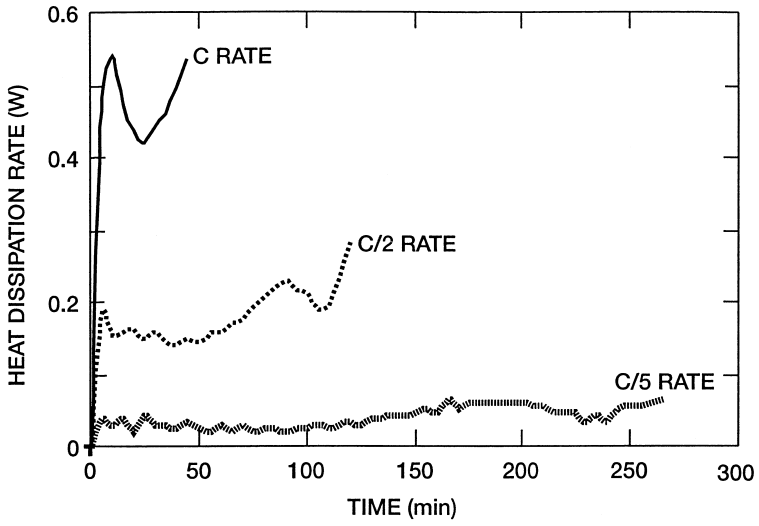

Fig. 9. Variation of heat rate at various rates of discharge for the 75% $LiCoO_2$, 25% $LiNiO_2$ cell.

obtained for the $Li_xC/LiNiO_2$ cell. A general value of 10 mW/cm^3 was reported by Chen et al. [5] based on mathematical calculations for a lithium ion cell.

The variation in heat dissipation rate for the $LiNiO_2$ cell during discharge at three different rates was determined, and the results are shown in Fig. 10. At 1 A rate of discharge, the heat dissipation profile showed an initial maximum of 0.3 W. The heat rate subsequently stabilized at 0.23 W before increasing to 0.6 W. This behavior was similar at 1.98 A discharge, where the heat rate stabilized to 0.8 W from an initial maximum of 1.04 W. At 3.59 A discharge, the initial maximum was 2.58 W and the stabilized value was 2 W. The heat dissipated at a medium rate of discharge was 17 mW/cm^3. Table 3 displays a short summary of the calorimetric data for the two types of cells which includes heat radiated and dissipated during discharge at the *C*/2 rate. The conductive correction for the smaller 75% $LiCoO_2$, 25% $LiNiO_2$ cell is larger, mainly due to the type of sense wires and thermocouple used.

The difference in the heat dissipation rates for the two types of cells at the *C*/2 rate of discharge could result from a number of cell construction features, such as the dimensions of the spirally wound electrode coil, the amount of electrolyte, and differences in the anode and cathode active material. Since graphite is the anode material in both cases, the cathode materials remain an important source for changes in heat dissipation at the anode. Thus, from the viewpoint of cell operation, there is an advantage in selecting $LiCoO_2$ as the cathode material.

The most striking feature of the heat dissipation is the initial maximum, followed by a reduction in the heat rate. The expected behavior was a gradual increase in the heat rate as discharge continued, followed by a very rapid rise towards the end of discharge.

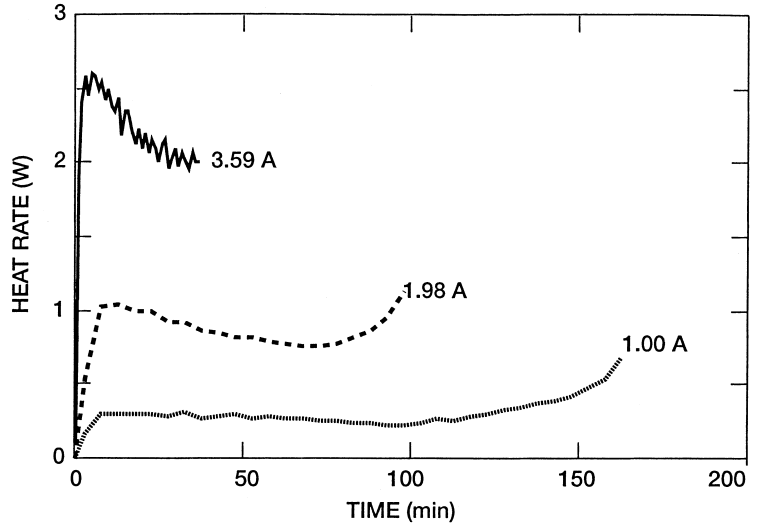

Fig. 10. Variation of heat dissipation rate with rate of discharge for the $LiNiO_2$ cell.

Table 3
Summary of calorimetric data for the two types of cathodes

Parameter	$LiNO_2$	75% $LiCoO_2$, 25% $LiNiO_2$
Heater area (cm^2)	26.7	12.9
Specific thermal capacity (J/°C)	111.5	40.246
Conductive correction, Q_c (W/°C)	0.00137	0.01118
Heat radiated at end of discharge at *C*/2 rate, Q_r (W)	1.59	1.193
Heat dissipated at end of discharge at *C*/2 rate, Q_{diss} (W)	1.13	0.285

The total heat generated in the cell is attributable to entropic effect, ohmic effect, and electrochemical polarization. The heat rate attributable to electrochemical polarization is expected to be much lower at the beginning of discharge, and to increase gradually. The entropic contribution is a function of the chemical state of the participants in the main cell reaction. Ohmic heating is assumed to exhibit no significant change during discharge and is expected to be lower than the heat due to entropy change. It is suggested that the initial increase in the heat rate during discharge is entropy-related. The main cell reaction is lithiation of the cathode, which is believed to be exothermic. The structure of Li_xCoO_2 and $LiNiO_2$ have been studied and are believed to undergo reversible phase transitions due to switching between trigonal and monoclinic crystal symmetries. Thackeray [9] has listed the lattice parameters as a function of lithium content in the Li_xNiO_2 structure and states that the monoclinic form exists from Li = 0.79 to Li = 0.49. Bernardi et al. [10] reported that phase changes contribute to the total enthalpy and included them as a separate term, in addition to reaction enthalpy and the enthalpy of mixing [10]. The suggested explanation for the initial increase, followed by minimum, in the heat rate curve is a phase change in the cathode active material.

9. Delayed heat evolution

The occurrence of nonfaradaic processes such as the chemical reaction of the electrolyte with the anode and cathode active material, phase changes in the cathode active material, and redistribution of lithium in the carbon anode can be inferred from the heat dissipation rates during open circuit periods following a discharge to 2.5 V. Fig. 11 shows the heat rates obtained for the Li_xC/75% $LiCoO_2$, 25% $LiNiO_2$ cell following completion of discharge at *C*/2 and *C* rates. Initially, the heat rate fluctuated and then stabilized in both cases to about 0.01 W. Although the heat rate is negligible, its occurrence points to a continuation of the processes.

10. Thermoneutral potential

The heat dissipation data obtained can be used to calculate the thermoneutral potential using

$$E_H = -\frac{Q_{diss}}{I} + E_L \quad (9)$$

where Q_{diss} is the heat dissipated (W, value is negative to indicate an exothermic reaction), E_H the thermoneutral

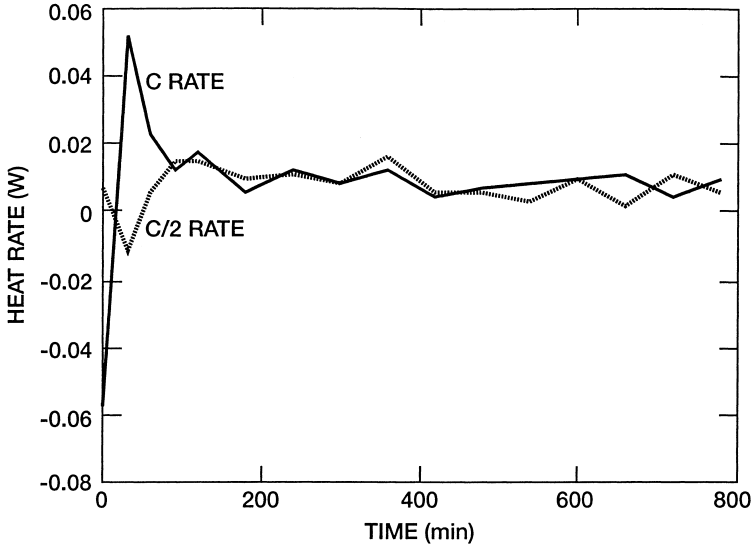

Fig. 11. Delayed heat after discharge for the 75% $LiCoO_2$, 25% $LiNiO_2$ cell.

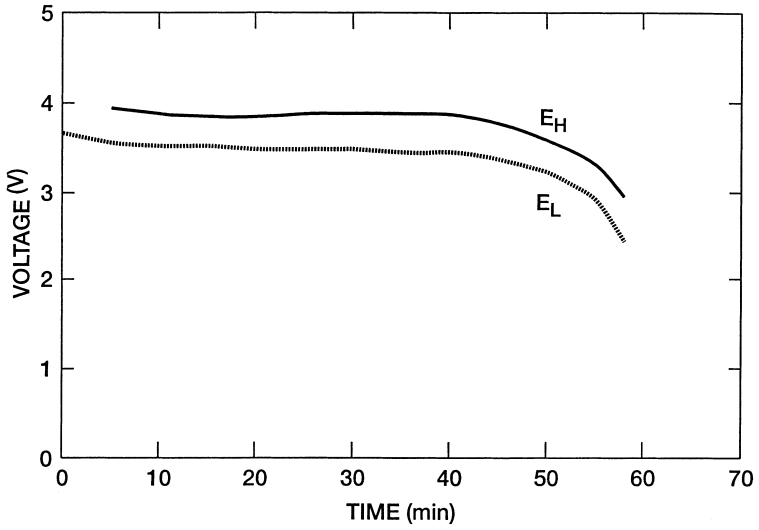

Fig. 12. Variation of E_H and E_L during discharge at 1 A for the $LiNiO_2$ cell.

potential (V), I the discharge current (A) and where E_L is the cell voltage during discharge (V).

This equation assumes that the discharge reaction is 100% efficient, and that parasitic reactions are neglected.

Fig. 12 shows the variation in thermoneutral potential for the $LiNiO_2$ cell as a function of state of charge during discharge at 1 A. The value for E_H, which varies from 3.726 to 4.09 V, was calculated during various rates of charge and discharge. Table 4 gives the values obtained. The average value calculated from the plateau is 3.698 V.

Fig. 13 shows the variation in calculated E_H for the 75% $LiCoO_2$, 25% $LiNiO_2$ cell during charge and discharge. The three curves that show the variation in E_H during discharge at $C/5$, $C/2$, and C rates have a plateau in the mid-discharge region. The values for E_H at different rates of discharge show some variability; however, the overall variability in the plateau region is negligible. The curve obtained during charge at $C/5$ shows very stable values for E_H. Table 4

Table 4
E_H values

Test regime	Value of E_H
(a) With 75% $LiCoO_2$, 25% $LiNiO_2$ cathode	
Discharge at 1 A	3.8073
Charge at $C/2$	3.8109
Discharge at $C/2$	3.8037
Charge at $C/5$ at 5°C	3.8456
Charge at $C/5$ at 18°C	3.8726
Discharge at C	3.8829
Discharge at $C/5$ at 5°C	3.8357
Average	3.8369
(b) With nickel-oxide cathode	
Discharge at $C/4$	3.8883
Charge at $C/10$	3.6657
Discharge at $C/2$	3.6039
Discharge at C	3.6350
Average	3.6982

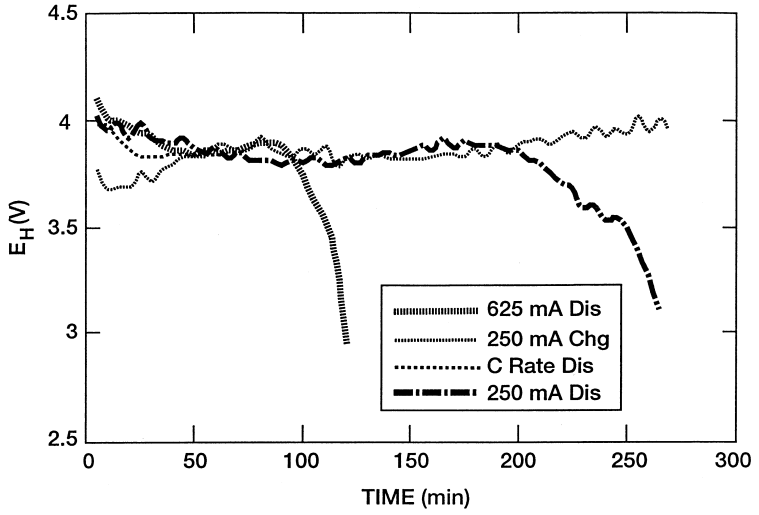

Fig. 13. Variation of E_H during discharge and charge for the 75% $LiCoO_2$, 25% $LiNiO_2$ cell.

displays the average values obtained under each condition. The overall average value from the calculation is 3.698 V. The values obtained in this study for the thermoneutral potential of the 75% $LiCoO_2$, 25% $LiNiO_2$ cell are in agreement with the negative temperature coefficient for the voltage reported in the literature [2,7]. It can be inferred from the thermoneutral potential that

- the products of the discharge reaction are more ordered than the reactants;
- endothermic cooling occurs at some point during charge;
- battery discharge will generate heat;
- open-circuit potential will be less than the thermoneutral potential at all temperatures.

Ordinarily, thermoneutral potential can be used to calculate heat dissipation under various operating conditions, based on a knowledge of the voltage profiles during charge and discharge. Before the values reported in this study are used, they should be confirmed using cells produced under various manufacturing conditions.

11. Conclusions

A radiative calorimeter was used to obtain experimental heat rate dissipation data on a 3.7 A h lithium ion cell based on an $LiNiO_2$ cathode, and a 1.25 A h cell based on a mixture of $LiCoO_2$ and $LiNiO_2$. The specific thermal capacity of the cells was determined experimentally to be 111.5 and 40. 24 J/°C for the $Li_xC/LiNiO_2$ cell and Li_xC/75% $LiCoO_2$, 25% $LiNiO_2$ cell, respectively. The heat dissipated during discharge increased with the rate of discharge. During charge, initial endothermic cooling and subsequent exothermic heating beyond 55% state-of-charge were observed. At the *C*/2 rate of discharge (which is considered a medium rate), the heat dissipated was 17 mW/cm^3 for the $Li_xC/LiNiO_2$ cell and 11.2 mW/cm^3 for the Li_xC/75% $LiCoO_2$, 25% $LiNiO_2$ cell. The difference in the heat dissipation rates is noteworthy and confirms the belief that reactions at the cathode contribute more to total heat than those at the anode. The heat dissipation profile during discharge is also characterized by a minimum that is different from that observed for Ni–Cd and Ni–H_2 cells. The minimum is attributed to phase changes in both the 75% $LiCoO_2$, 25% $LiNiO_2$ and $LiNiO_2$ cells.

Experimental values obtained for heat dissipation at various charge and discharge rates were used to calculate thermoneutral potential values of 3.698 and 3.836 V for $Li_xC/LiNiO_2$ and Li_xC/75% $LiCoO_2$, 25% $LiNiO_2$ cells, respectively. The proposed values for thermoneutral potential can explain the endothermic cooling observed during charge, as well as the negative temperature coefficient for cell voltage. The self-discharge rate for the Li_xC/75% $LiCoO_2$, 25% $LiNiO_2$ cell was lower than for the $Li_xC/LiNiO_2$ cell. Thus, two important selection parameters — heat rate during discharge and self-discharge rate — favor the use of $LiCoO_2$ over $LiNiO_2$ as the cathode material for lithium ion cells.

Acknowledgements

The authors would like to thank R. Clark for performing the calorimetric measurements.

References

[1] T. Nagura, in: Proceedings of the 4th International Rechargeable Battery Seminar, Deerfield Beach, FL, 1990.
[2] J.R. Dahn, A.K. Sleigh, H. Shi, B.M. Way, W.J. Weydanz, J.N. Reimers, Q. Zhong, Von Sacken, in: G. Pistoia (Ed.), Lithium Batteries, Chapter 1, Industrial Chemistry Library, Vol. 5, Elsevier, Amsterdam (London), 1994.
[3] G. Nagasubramanian, R.G. Jungst, D. Ingersoll, D.H. Doughty, in: Proceedings of the 38th Power Sources Conference, Cherry Hill, NJ, 1998, p. 493.
[4] B.V. Ratnakumar, M.C. Smart, S. Surampudi, in: Proceedings of the 38th Power Sources Conference, Cherry Hill, NJ, 1998, p. 503.
[5] Y. Chen, J.W. Evans, J. Electrochem. Soc. 143 (1996) 2708.
[6] J.-S. Hong, H. Maleki, S. Al Hallaj, L. Redey, J.R. Selman, J. Electrochem. Soc. 145 (1998) 1489.
[7] E. Deiss, A. Wokaun, J.-L. Barras, C. Daul, P. Dufek, J. Electrochem. Soc. 144 (1977) 3877.
[8] H. Vaidyanathan, W.H. Kelly, in: Proceedings of the Intersociety Energy Conversion Engineering Conference, San Diego, CA, Vol. 1, Society of Automobile Engineers, Warrendale, PA, 1992, p. 209.
[9] M.M. Thackeray, J. Electrochem. Soc. 142 (1995) 2538.
[10] D. Bernardi, E. Pawlikowski, J. Newman, J. Electrochem. Soc. 132 (1985) 5.